

# UniAR: Unifying Human Attention and Response Prediction on Visual Content

Peizhao Li<sup>\*†1</sup>, Junfeng He<sup>\*‡2</sup>, Gang Li<sup>\*‡2</sup>, Rachit Bhargava<sup>2</sup>, Shaolei Shen<sup>2</sup>, Nachiappan Valliappan<sup>2</sup>, Youwei Liang<sup>†3</sup>, Hongxiang Gu<sup>2</sup>, Venky Ramachandran<sup>2</sup>, Golnaz Farhadi<sup>2</sup>, Yang Li<sup>2</sup>, Kai J Kohlhoff<sup>2</sup>, and Vidhya Navalpakkam<sup>2</sup>

<sup>1</sup>Brandeis University

<sup>2</sup>Google Research

<sup>3</sup>University of California San Diego

## Abstract

*Progress in human behavior modeling involves understanding both implicit, early-stage perceptual behavior such as human attention and explicit, later-stage behavior such as subjective ratings/preferences. Yet, most prior research has focused on modeling implicit and explicit human behavior in isolation. Can we build a unified model of human attention and preference behavior that reliably works across diverse types of visual content? Such a model would enable predicting subjective feedback such as overall satisfaction or aesthetic quality ratings, along with the underlying human attention or interaction heatmaps and viewing order, enabling designers and content-creation models to optimize their creation for human-centric improvements. In this paper, we propose UniAR – a unified model that predicts both implicit and explicit human behavior across different types of visual content. UniAR leverages a multi-modal transformer, featuring distinct prediction heads for each facet, and predicts attention heatmap, scanpath or viewing order, and subjective rating/preference. We train UniAR on diverse public datasets spanning natural images, web pages and graphic designs, and achieve leading performance on multiple benchmarks across different image domains and various behavior modeling tasks. Potential applications include providing instant feedback on the effectiveness of UIs/digital designs/images, and serving as a reward model to further optimize design/image creation.*

## 1. Introduction

Implicit, early-stage perceptual behavior such as human attention is intricately linked with explicit, later-stage behavior such as subjective ratings/preferences. Yet, prior research has often studied these in isolation. For example, there’s a large body of work on predictive models of human attention that are known to be useful for various applications, ranging from optimizing interaction designs [4, 9, 58], enhancing web page layouts [11, 60, 76], to improving user experience in immersive environments [5] and improving natural images by minimizing distracting regions [1]. In addition to predicting attention heatmaps (that are a probability distribution over human gaze), there have also been efforts to predict other kinds of implicit human behavior such as the sequence/order in which items are viewed (attention scanpath) in natural images or web pages [20, 23], assessing visual importance in graphic designs [26, 42, 56], and understanding visual clutter [46, 63, 70].

Separately from implicit behavior, there’s also been research in modeling explicit, subjective feedback such as human preferences [21], and aesthetic quality ratings [29, 49]. Prior research has been further fragmented due to focusing on specific tasks within a single domain, and typically under constrained scenarios such as free-viewing, object search, or question answering (e.g., predicting attention heatmaps for free-viewing images, or annotations for object search).

To the best of our knowledge, there doesn’t exist a unified approach to modeling both implicit and explicit behavior, ranging from early-perceptual behavior of what catches attention to later-stage decision-making on subjective ratings/preferences. In this paper, we try to answer the following question: *Can we build a unified model of human attention and preference behavior that reliably works across diverse types of visual content? If so, how does it compare with state-of-the-art (SOTA) models dedicated to specific*

<sup>\*</sup>Co-first authors, equal technical contribution

<sup>†</sup>The work is done during an internship at Google

<sup>‡</sup>Corresponding authors, equal leading contribution:

{junfenghe, leebird}@google.com

*domain/task?* Such a model could enable a wide variety of applications. For instance, it could act as a comprehensive reward model, that would not only predict subjective ratings/preferences as rewards, but also provide additional insights from predicted human attention and behavior patterns, serving as a rationale for the assigned reward scores.

**UniAR** In this paper, we consider 10 public datasets encompassing saliency, scanpath, and rating prediction, spanning digital designs and natural scenes for unified modeling. We introduce a multimodal model, **UniAR** (Unifying User Attention and Response), which takes as input both image and text prompts. The text prompt combines information about the input domain (e.g., natural image or web pages), the desired output prediction type (e.g., aesthetic score or scanpath), and specifics of the task scenario when relevant (e.g., object name in an object search task). UniAR generates predictions corresponding to these diverse inputs. Experiments show that UniAR achieves leading performance across all datasets, regardless of input domains, output prediction types, and task scenarios. Additionally, UniAR exhibits notable generalization capabilities: it performs well in zero-shot settings, making accurate predictions even when data from the target domain or task is not available, relying instead on related domains or tasks.

**Main contributions** of this work are summarized below:

1. We proposed UniAR, a unified multimodal transformer model to predict both implicit and explicit human behavior across diverse types of visual content and tasks.
2. We trained UniAR on 10 benchmark datasets with different input domains (natural scenes/web pages/graphic designs) and output types (attention/importance heatmaps, sequence of viewing or scanpath, aesthetics/quality scores), and showed that UniAR, which is a single unified model can outperform or perform comparably to SOTA models on all the datasets. We further showed that UniAR generalizes well to tasks with unseen input and output combinations, under a zero-shot setting.

## 2. Related Work

We describe some recent works in saliency, scanpath, and rating prediction, then highlight our uniqueness.

**Saliency prediction** Saliency prediction is to identify the most visually significant or attention-grabbing area within an image. Such predictions can be crucial for enhancing user interfaces, optimizing content placement in graphic designs, and improving the perceptual quality of compressed images or videos. By allocating more resources to these salient regions, one can maintain vital information while compressing the less significant parts to reduce bandwidth.

The current general solution is to use Convolutional Neural Networks as the backbone model to predict the

Gaussian-blurred 2D heatmap, which aggregates all fixations from multiple observers [12, 19, 33, 40, 55]. Customized modules, such as  $1 \times 1$  read-out convolutions [33] and Attentive ConvLSTM [19], have been introduced atop these CNNs to boost performance. Instead of the heatmap, regressing the Gaussian probability distribution is also demonstrated as an alternative way for fixation predictions [55]. Some work also investigates the feature contributions to saliency prediction and confirms the usage of low-level features [40]. Expanding the scenarios, Chen et al. [17] addresses the challenge of predicting attention heatmaps in scenarios where users are tasked with identifying missing objects in images, and Chen et al. [12] propose to incorporate user profile information to personalize saliency predictions in each individual user case.

**Scanpath prediction** Scanpath prediction aims to forecast the trajectory of human eye movements as they engage with image content, offering insights into how individuals observe and comprehend visual information. With web pages as an example, predicting scanpaths on web pages can inform the optimal arrangement of information or advertisements, ensuring priority content captures attention first; this has implications for dynamic storytelling as well.

Previous research has worked on scanpath predictions within various aspects of the human gaze, including free-viewing scanpath prediction, object searching, and visual question answering, utilizing deep learning approaches. Yang et al. [68] introduce a method utilizing inverse reinforcement learning for scanpath prediction in the context of visual object searching. Continuing with this framework, Yang et al. [69] propose the concept of Foveated Feature Maps within the framework of inverse reinforcement learning, enabling the prediction of scanpath when users seek an object that is not present in the initial image. To facilitate the understanding of the instruction when performing a visual search over the image, Chen et al. [14] propose the use of a visual-question-answering model combined with a ConvLSTM module to predict the distribution of fixation positions and duration in response to a question regarding the associated natural image. With the development of Transformer, Mondal et al. [48] propose employing the Transformer model to regress coordinates for each fixation within a scanpath dedicated to object searching. This regression is conditioned on the embedding of the object’s name from a pre-trained language model.

**Subjective rating prediction** Predicting the subjective rating from humans can help to better assess image quality and enhance graphic design. The continuous or discrete rating may reflect both the technical quality and aesthetic quality of an image, and it is the most direct quantitative evaluation to use in subsequent applications. Statistic-based methods [47, 74] and Convolutional Neural Networks-based

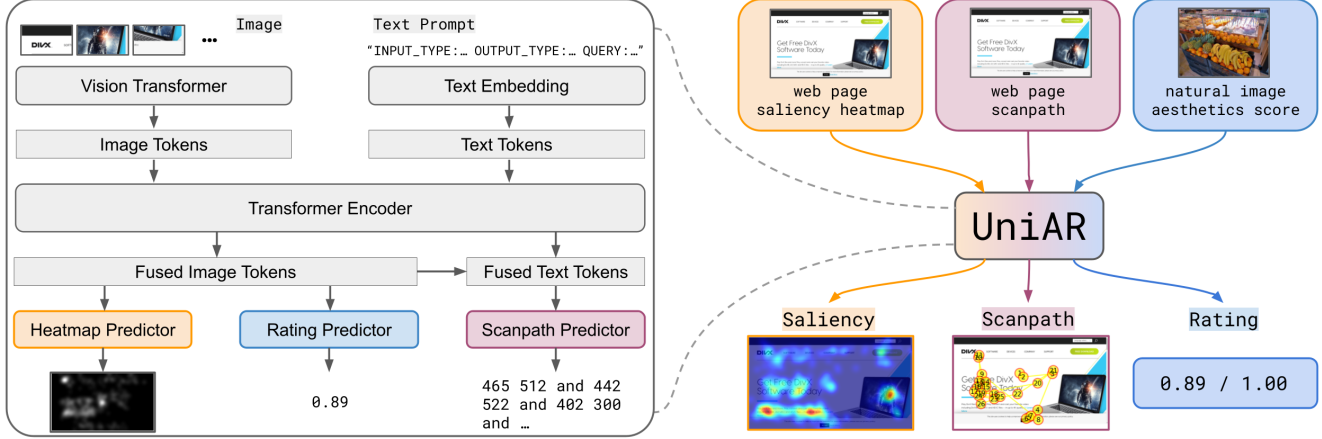


Figure 1. Overview of our UniAR model. UniAR is a multimodal model that takes an image (could be a natural scene, a screenshot of a web page, graphic design, or UI) along with a text prompt as input, and outputs heatmaps of human attention/interaction, scanpath or sequence of viewing/order, and subjective ratings/preference. Example inputs and corresponding outputs are shown on the right side.

methods [61, 75] are proposed, and recently Vision Transformer is also adopted for this task [36].

**Multi-tasking Unified Model** Most recently, there have been many large model developments in natural language processing [3, 18, 51] and vision-language learning [15]. These works fine-tune large models (basically Transformer models) on datasets containing a series of recognition and reasoning tasks such as text summarization, sentiment analysis, machine translation for language models, and image captioning, question-answering, detection for vision-language models. These fine-tuned large models show strong generalization capacity across various tasks. Our research is motivated by the class of generalized and unified large models, and intend to develop the first unified model UniAR for human behavior modeling on visual content.

In line with this ongoing work on saliency, scanpath, and rating research, instead of task-dedicated or domain-dedicated modeling, our work seeks unified and generalized modeling of these user-centered prediction tasks.

### 3. Unifying User Attention and Response

We illustrate the overall model architecture along with example inputs, and corresponding outputs in Fig. 1.

#### 3.1. Model Architecture

We adopt a multimodal encoder-decoder transformer model to unify the various human behavior modeling tasks. The model takes two types of inputs: an image and a text prompt. Its architecture comprises several components: a Vision Transformer model [24] for image encoding, a word embedding layer to embed text tokens, and a T5 [54] Transformer encoder to fuse image and text representations. Additionally, it has three separate predictors: a heatmap predictor for attention/saliency heatmaps or visual importance heatmaps, a scanpath predictor for the sequence/order of

viewing, and a rating predictor for quality/aesthetic scores of images or web pages. These predictors are described in Secs. 3.3 to 3.5. Besides the architecture, the text prompt is designed to encode relevant information about the input domain, the expected prediction type of the model, and other task-related information such as viewing scenarios (e.g., free-viewing, object-searching), target object names, or questions to be answered, as described in Sec. 3.6.

More details about model architecture such as the number of layers and layer size can be found in Appendix A.

#### 3.2. Backbone

We adopt Spotlight [45] as our backbone, and make two key modifications for our specific needs. **(1) Dataset expansion:** The original Spotlight model is pre-trained on large-scale web page and mobile interface data only. To diversify the data and broaden the model’s applicability for natural scene images, we augment the pre-training datasets with WebLI [15] natural image captioning datasets for our backbone model. To support tasks requiring coordinate prediction such as scanpath prediction, we also add a pretraining task to predict bounding box coordinates given a text snippet and the screenshot in the web page and mobile interface data. **(2) Module replacement:** We replace the cross-attention module between the vision and text tokens in Spotlight with a Transformer encoder, as in PaLI [15]. This is more suitable for our tasks as we need to propagate information in both directions, e.g., input and output information from text tokens to image tokens, and vision information from image tokens to text tokens for better vision-aware text encoding for tasks such as predicting scanpath and viewing order for object-searching on visual content.

#### 3.3. Heatmap Predictor

Our model incorporates a heatmap head which is commonly used in attention/saliency research (e.g., predicting

probability distribution of gaze over the input image). The heatmap prediction head takes the fused image tokens after the Transformer encoder, and processes the features via several read-out convolution layers, together with up-sampling so that the output will match the resolution of the input image. A sigmoid function is used at the end to ensure the generated values fall within the range  $[0, 1]$  for each pixel.

In the experiments, we consider two kinds of heatmap, namely saliency and importance heatmap. A saliency heatmap is generated via aggregating human fixation points from multiple participants viewing an image. This heatmap is gathered through user studies on visual content and eye-tracking techniques. On the other hand, importance heatmaps are annotated by manual region selection to highlight the most critical design elements in a graphic design [25]. Each of these heatmaps reflects distinct aspects of human attention and preference/annotation.

To differentiate these two types of heatmaps within a single heatmap prediction head, we use the text prompt to specify the type of heatmap that the model is expected to generate for the given input sample. Such a design enables supporting a variety of heatmap prediction tasks (e.g., attention, interaction, importance, etc.) with a single heatmap prediction head. We adopt a pixel-wise  $\ell_2$  loss function for the heatmap predictor during training.

### 3.4. Scanpath (Sequence) Predictor

The scanpath predictor takes both the fused image and text tokens after the Transformer encoder as input, and applies a Transformer decoder to generate the predicted scanpath.

A scanpath is defined as a sequence of 2D locations  $(x_1, y_1), (x_2, y_2), \dots, (x_N, y_N)$  with a total of  $N$  fixations, capturing the temporal aspect of attention and visual exploration. The subsequent fixations are conditional on all the previous fixations, thus fitting an autoregressive model with conditional generation. Inspired by previous literature, we use Transformer decoder for object detection and other localization tasks [13, 45], and therefore generate the location end-to-end with Transformer and text generation. In general, we let the Transformer predict the sequence of coordinates as characters in a string one after one and readout the locations from the generated text subsequently.

We spatially decompose the entire image into  $1,000 \times 1,000$  bins with equal interval, and map each coordinate  $x_n$  or  $y_n$  to its nearest bin  $\tilde{x}_n, \tilde{y}_n \in \mathbb{Z}$  in the range  $[0, 999]$ .

To formulate the target sequence for teacher-forcing training, we put a special token ‘`<extra_id_01>`’ at the start of each target sequence, and attach another special token ‘`<extra_id_02>`’ at the end, to indicate the entire scanpath sequence. We concatenate location coordinates with a separation word ‘and’. Let  $y$  indicate the target sequence with length  $3N + 1$  with  $N$  fixations, we have the target sequence for teacher-forcing training as follows ( $\rightarrow$

indicates the line changing due to the paper format):

$$y = \text{<extra\_id\_01>} \ \tilde{x}_1 \ \tilde{y}_1 \ \text{and} \ \tilde{x}_2 \ \tilde{y}_2 \ \text{and} \ \dots \\ \rightarrow \text{and} \ \tilde{x}_N \ \tilde{y}_N \ \text{<extra\_id\_02>}.$$

The training objective is to maximize the log-likelihood of tokens conditioned on the input image and all preceding tokens in ground-truth scanpath string, i.e.,

$$\max \sum_{j=1}^{3N+1} w_j \log P(\tilde{y}_j | x, y_{1:j-1}), \quad (1)$$

where  $x$  is the input image and text prompt, and  $y$  is the target sequence associated with  $x$ .  $w_j$  is the weight for the  $j$ -th token that can adapt weights for different types of tokens. We use a unified weight for each token in experiments.

**Decoding during inference** During inference, it is not strictly guaranteed that the generated string will exactly follow the format of the target sequence, especially when the number of fixations is relatively large (e.g.,  $N \geq 30$ ), resulting in an invalid sequence to readout. To deal with the possible invalid cases, in practice, we identify the two special tokens ‘`<extra_id_01>`’ and ‘`<extra_id_02>`’ in the predicted string if available, and extract the context between these two special tokens. Then we split the extracted string with the separator word ‘and’. For a pair of two tokens from the beginning, we check if they are both numerical. If so, we add one fixation with this coordinate after mapping them to the original resolution, then iteratively move to the following, and if not, we terminate the decoding process and keep the existing sequence. If there is no fixation available in the predicted string, we mark the scanpath as invalid. During training, we observe that the validation rate (#valid scanpaths / #all scanpaths generated) of scanpath decoding quickly converges to 1, meaning every predicted scanpath will contain valid fixation(s).

Compared to the scanpath predictors in GazeFormer [48] which predicts each point as 2D continuous numbers instead of two text tokens, our model seems less intuitive. However, as shown in Sec. 4.3, the proposed scanpath predictor works quite well. Moreover, one advantage of the current design of the scanpath predictor is that it can be easily extended to predict human responses of other kinds of sequences too, e.g., text sequence, or 1-D number sequence, with just some modifications on the sequence output format. This flexibility is important for a unified model like ours.

### 3.5. Rating Predictor

We take a simple prediction head which takes image tokens after the Transformer encoder module, and processes the features via a few convolution and connected layers. An  $\ell_2$  loss is used for training the rating predictor with rating data.

Table 1. List of all public datasets used to train our model. ‘# Image’ denotes the number of unique images in the entire dataset. Note that for annotation ‘scanpath,’ there are multiple scanpaths recorded from a group of users associated with one image, so ‘# Training Sample’ is much larger than ‘# Image.’ During training, we randomly sample from all training datasets with an equal sampling rate.

Dataset	Image domain	Training annotation	Viewing style	# Image	Image Resolution	# Training Sample
<i>Salicon</i> [34]	Natural scene	Saliency heatmap	Free-viewing	15,000	640 × 480	10,000
<i>OSIE</i> [65]	Natural scene	Saliency heatmap	Free-viewing	700	800 × 600	500
<i>WS-Saliency</i> [11]	Web page	Saliency heatmap	Free-viewing	450	1,280 × 720	392
<i>Mobile UI</i> [42]	Mobile user interface	Saliency heatmap	Free-viewing	193	Varied	154
<i>Imp1k</i> [25]	Graphic design	Importance heatmap	N/A	998	Varied	798
<i>WS-Scanpath</i> [11]	Web page	Scanpath	Free-viewing	450	1,280 × 720	5,448
<i>FiWI</i> [60]	Web page	Saliency	Free-viewing	159	1,360 × 768	121
<i>COCO-Search18</i> [16]	Natural scene	Scanpath	Object-searching	3,101	1,680 × 1,050	21,622
<i>COCO-FreeView</i> [16]	Natural scene	Scanpath	Free-viewing	3,101	1,680 × 1,050	37,038
<i>KoniQ-10k</i> [30]	Natural scene	Rating	N/A	10,073	1,280 × 720	7,000
<i>Web Aesthetics</i> [22]	Web page	Rating	N/A	398	1,280 × 768	398

### 3.6. Text Prompt

To enhance the model’s ability to generalize across a variety of visual content and usage scenarios, we integrate specific task instructions into the model via text prompts. The prompts used in UniAR are structured as follows:

```
INPUT_TYPE:<input_type>
OUTPUT_TYPE:<output_type>
QUERY:<query>
```

We fill `<input_type>` with string taken from `{natural image | web page | graphic design | mobile user interface}` and `<output_type>` taken from `{saliency heatmap | importance heatmap | aesthetics score | scanpath}`. We append a query in string `Query:<query>` to the prompt if a task-specific query is available, for example, the object name to search, or the question to answer, depending on the use case. The prompt we use is modularized and can easily adapt to different types of datasets and scenarios.

## 4. Experiment

### 4.1. Protocol

**Datasets** Please refer to Tab. 1 for all public datasets we consider in training and benchmarking. For more dataset processing details, please refer to Appendix B.

**Benchmarks** We reuse benchmarks from recent literature for model comparison purposes. We adopt the benchmarks for *WS-Saliency* and *WS-Scanpath* from Tab. 3 and 7 in Chakraborty et al. [11] respectively, *Mobile UI* from Tab. 2 in Leiva et al. [42], *Imp1k* from Tab. 2 in Fosco et al. [25], *OSIE* from Tab. 4 in Chen et al. [12], *Salicon* from Tab. 1 in Reddy et al. [55], *COCO-Search18* from Tab. 1 in Mondal et al. [48], *KoniQ-10k* from Tab. 2 in Ke et al. [36], and *Web Aesthetics* from Tab. 4 in Delitzas et al. [22].

**Evaluation metrics** Inheriting from the above benchmarks, we consider the following evaluation metrics.

**CC** [41]: Pearson’s Correlation Coefficient is used here

to measure the linear relationship in all pixel values between the predicted and ground-truth saliency heatmaps; **KLD** [38]: the metric to use KL-Divergence between the predicted heatmap and ground-truth heatmap to measure the distribution discrepancy, with the prediction used as the target distribution. **AUC-Judd** [35]: Area under ROC curve (AUC) in the variant from Judd et al. [35] treating the heatmap prediction as binary classification with various thresholds. The specific calculations of true positive and false positive rates can be referred to [10]. **SAUC** [6]: the shuffled AUC metric samples negatives from other images for AUC calculation. **NSS** [53]: Normalized Scanpath Saliency is the average saliency strength (pixel values in the predicted heatmap) at all ground-truth fixation locations. **SIM** [57]: Similarity is computed as the sum of the minimum values among the normalized prediction and ground-truth heatmaps. **RMSE**: the root mean square error between the predicted and ground-truth heatmaps. **R-Squared ( $R^2$ )**: the coefficient of determination applied to all values in the heatmap. **SemSS** [69]: Semantic Sequence Score converts each fixation to an ID decided by a semantic segmentation over the image, and compares two strings with a string-matching algorithm [50]. **SemFED** [69]: similar to SemSS, Semantic Fixation Edit Distance uses Levenshtein distance for string matching [43]. **SequenceScore**: similar to SemSS, but instead of using a semantic segmentation map, the Sequence Score uses the clustering results from a MeanShift clustering to segment the image and map the fixation to their ID. **MultiMatch** [23]: MultiMatch is the average of four metrics of scanpath, namely: **Shape**, **Direction**, **Length**, and **Position**, characterizing the similarity between the predicted scanpath and its ground-truth. **SRCC** and **PLCC**: refer to Spearman’s rank correlation coefficient and Pearson’s linear correlation coefficient, respectively, used to quantify the quality of predicted ratings.

Experimental benchmarks for one task among different datasets may not have uniform evaluation metrics but most of their metrics are shared. For saliency and importance heatmap predictions, we resize the predicted heatmap back

Table 2. Heatmap prediction results on five public datasets spanning digital design and natural scene, benchmarking with eight metrics in total. The details on datasets and evaluation metrics can be found in Sec. 4.1. For *Imp1k* dataset we predict the importance heatmap, while for the rest of the four datasets, we predict attention/saliency heatmap. Our method is highlighted with green background. For each dataset and each metric, the best result in the current column is in **bold**, and the second best result is in **blue**. For our model, the relative performance change compared to the second best result (or the best result if we are not the best) in % is noted.

Dataset	Method	CC $\uparrow$	KLD $\downarrow$	AUC-Judd $\uparrow$	sAUC $\uparrow$	SIM $\uparrow$	NSS $\uparrow$	RMSE $\downarrow$	$R^2 \uparrow$
Mobile UI [42] (Mobile interface)	Itti et al. [32]	0.082	-	0.223	-	0.558	0.126	-	-
	BMS [73]	0.131	-	0.249	-	0.206	0.138	-	-
	GBVS [27]	0.580	-	0.666	-	0.709	0.591	-	-
	ResNet-Sal [42]	0.657	-	0.692	-	0.734	0.704	-	-
	SAM-S2015 [19]	0.477	-	0.650	-	0.562	0.537	-	-
	SAM-S2017 [19]	<b>0.834</b>	-	<b>0.723</b>	-	<b>0.819</b>	<b>0.839</b>	-	-
	SAM-mobile [42]	0.621	-	0.666	-	0.664	0.655	-	-
Unified Model - Ours		<b>0.871</b> +4.44%	<b>0.120</b> +0.00%	<b>0.756</b> +4.56%	-	<b>0.826</b> +0.85%	<b>1.001</b> +19.31%	<b>0.121</b> +0.00%	<b>0.763</b> +0.00%
WS-Saliency [11] (Web page)	Itti et al. [32]	0.367	0.840	0.710	0.661	-	0.769	-	-
	Deep Gaze II [39]	0.574	3.449	0.815	0.644	-	1.380	-	-
	SalGAN + WS [52]	0.637	0.622	0.818	0.703	-	1.458	-	-
	DVA [64]	0.571	0.701	0.805	0.711	-	1.260	-	-
	UAVDVSM [28]	0.519	0.858	0.739	0.668	-	1.133	-	-
	SAM-ResNet [19]	0.596	1.506	0.795	0.717	-	1.284	-	-
	EML-NET [33]	0.565	2.110	0.790	0.702	-	1.277	-	-
	UMSI [25]	0.444	1.335	0.757	0.698	-	1.042	-	-
	TaskWebSal-FreeView [76]	0.525	0.784	0.769	0.714	-	1.107	-	-
	SAM-ResNet + WS [19]	0.718	0.994	0.828	0.725	-	1.532	-	-
	DI Net + WS [67]	0.798	0.690	0.852	0.739	-	1.777	-	-
	AGD-F (W/o-L) [11]	<b>0.815</b>	<b>0.637</b>	<b>0.858</b>	<b>0.753</b>	-	<b>1.802</b>	-	-
Unified Model - Ours		<b>0.836</b> +2.58%	<b>0.287</b> -54.95%	<b>0.863</b> +0.58%	<b>0.783</b> +3.98%	<b>0.744</b> +0.00%	<b>1.792</b> -0.55%	<b>0.084</b> +0.00%	<b>0.705</b> +0.00%
FiWI [60] (Web page)	DeepGaze II [39]	0.488	-	0.797	0.625	-	1.229	-	-
	SAM-ResNet [19]	0.595	-	0.791	0.673	-	1.246	-	-
	UMSI [25]	0.457	-	0.755	0.675	-	0.938	-	-
	AGD-F [11]	<b>0.735</b>	-	<b>0.767</b>	<b>0.748</b>	-	1.606	-	-
	EML-NET [33]	0.661	0.603	0.847	0.675	-	1.653	-	-
	EML-NET + Salicon [33]	0.689	0.567	0.848	0.697	-	1.722	-	-
	Chen et al. [12]	0.699	<b>0.564</b>	<b>0.851</b>	0.704	-	<b>1.752</b>	-	-
Unified Model - Ours		<b>0.740</b> +0.68%	<b>0.537</b> -4.79%	<b>0.861</b> +1.18%	<b>0.783</b> +4.68%	-	<b>1.855</b> +5.88%	-	-
Salicon [34] (Natural scene)	SalGAN [52]	0.763	-	-	<b>0.755</b>	-	-	-	-
	FastSal w. MobileNetV2 [31]	0.8751	-	0.845	0.736	-	1.816	-	-
	SimpleNet w. ResNet-50 [55]	0.895	0.211	0.868	-	0.786	1.881	-	-
	SimpleNet w. PNASNet-5 [55]	<b>0.907</b>	<b>0.193</b>	<b>0.871</b>	-	<b>0.797</b>	<b>1.926</b>	-	-
	MDNSal [55]	0.899	<b>0.217</b>	0.868	-	<b>0.797</b>	1.893	-	-
	Unified Model - Ours	<b>0.901</b> -0.66%	<b>0.215</b> +11.40%	<b>0.870</b> -0.11%	<b>0.752</b> -0.40%	<b>0.792</b> -0.63%	<b>1.947</b> +1.09%	<b>0.077</b> +0.00%	<b>0.813</b> +0.00%
OSIE [62] (Natural scene)	SALICON [34]	0.685	0.575	0.846	-	0.600	1.641	-	-
	SAM-ResNet [19]	0.758	<b>0.480</b>	<b>0.860</b>	-	<b>0.648</b>	1.811	-	-
	UMSI [25]	0.746	0.513	0.856	-	0.631	1.788	-	-
	EML-NET [33]	0.717	0.537	0.854	-	0.619	1.737	-	-
	Chen et al. [12]	<b>0.761</b>	<b>0.506</b>	<b>0.860</b>	-	<b>0.652</b>	<b>1.840</b>	-	-
	Unified Model - Ours	<b>0.754</b> -0.92%	0.547 +13.96%	<b>0.867</b> +0.81%	<b>0.739</b> +0.00%	0.647 -0.46%	<b>1.842</b> +0.11%	<b>0.100</b> +0.00%	<b>0.575</b> +0.00%
Imp1k [25] (Graphic design)	Bylinskii et al. [8]	0.758	0.301	-	-	-	-	0.181	0.072
	Bylinskii et al. [8]	0.732	0.388	-	-	-	-	0.205	0.061
	SAM [19]	0.866	0.166	-	-	-	-	0.168	0.108
	UMSI-nc [25]	0.802	0.177	-	-	-	-	0.152	0.095
	UMSI-2stream [25]	0.852	0.168	-	-	-	-	0.141	0.105
	UMSI [25]	<b>0.875</b>	<b>0.164</b>	-	-	-	-	<b>0.134</b>	<b>0.115</b>
	Unified Model - Ours	<b>0.904</b> +3.31%	<b>0.123</b> -25.00%	-	-	<b>0.845</b> +0.00%	-	<b>0.079</b> -41.04%	<b>0.823</b> +415.65%

Table 3. Scanpath prediction results on natural scene and digital design datasets, with object-searching and free-viewing tasks.

Dataset	Method	SemSS $\uparrow$	SemFED $\downarrow$	Sequence Score $\uparrow$	Shape $\uparrow$	Direction $\uparrow$	Length $\uparrow$	Position $\uparrow$	MultiMatch $\uparrow$
COCO-Search18 [16] (Natural scene, object searching)	IRL [68]	0.481	2.259	-	0.901	0.642	0.888	0.802	0.833
	Chen et al. [14]	0.470	<b>1.898</b>	-	0.903	0.591	0.891	0.865	0.820
	FFM [69]	0.407	2.425	-	0.896	0.615	<b>0.893</b>	0.850	0.808
	Gazeformer [48]	<b>0.496</b>	<b>1.861</b>	-	<b>0.905</b>	<b>0.721</b>	0.857	<b>0.914</b>	<b>0.849</b>
	Unified Model - Ours	<b>0.521</b> +5.04%	2.004 +7.68%	-	<b>0.946</b> +4.53%	<b>0.724</b> +0.42%	<b>0.924</b> +3.47%	<b>0.901</b> -1.42%	<b>0.874</b> +2.94%
WS Scanpath [11] (Web page, free-viewing)	Itti et al. [32]	-	-	0.177	0.781	0.676	0.778	0.594	0.707
	MASC [2]	-	-	0.169	0.788	0.580	0.818	0.514	0.717
	SceneWalker [59]	-	-	0.194	<b>0.843</b>	0.616	<b>0.842</b>	0.562	0.716
	G-Eymol [71]	-	-	0.218	0.820	0.673	0.816	0.681	0.748
	AGD-F (w. layout) [11]	-	-	0.203	0.787	0.642	0.771	0.677	0.719
	AGD-S (w/o layout) [11]	-	-	0.221	0.814	0.663	0.805	0.698	0.745
	AGD-S (w. layout) [11]	-	-	<b>0.224</b>	0.820	<b>0.677</b>	0.813	<b>0.708</b>	<b>0.755</b>
Unified Model - Ours		-	-	<b>0.267</b> +19.20%	<b>0.967</b> +14.71%	<b>0.826</b> +22.01%	<b>0.960</b> +14.01%	<b>0.794</b> +12.15%	<b>0.887</b> +17.48%

Table 4. Subjective rating prediction results on natural scene image dataset *KonIQ-10k* and web page dataset *Web Aesthetics*.

Dataset	Method	SRCC $\uparrow$	PLCC $\uparrow$
<i>KonIQ-10k</i> [30] (Natural scene)	BRISQUE [47]	0.665	0.681
	ILNIQE [74]	0.507	0.523
	HOSA [66]	0.671	0.694
	BIECON [37]	0.618	0.651
	WADIQaM [7]	0.797	0.805
	PQR [72]	0.880	0.884
	SFA [44]	0.856	0.872
	DBCNN [75]	0.875	0.884
	MetalQA [77]	0.850	0.887
	BIQA (25 crops) [61]	<b>0.906</b>	0.917
<i>Web Aesthetics</i> [22] (Web page)	MUSIQ-single [36]	<b>0.905</b>	<b>0.919</b>
	Ours	<b>0.905</b> <small>-0.11%</small>	<b>0.925</b> <small>+0.65%</small>
	Rating-based Calista [22]	-	0.770
	Comparison-based Calista [22]	-	<b>0.820</b>
	Ours	<b>0.813</b> <small>+0.00%</small>	<b>0.841</b> <small>+2.56%</small>

Table 5. Experiment on zero-shot generalization to *WS-Scanpath* dataset, described in Sec. 4.4. CC = *COCO-FreeView* dataset.

Training Set	Sequence Score $\uparrow$	MultiMatch $\uparrow$
<i>WS-Scanpath</i> (SOTA results from [11])	0.224	0.755
<i>WS-Scanpath</i> (ours)	0.261	0.894
UniAR full model	0.267	0.887
CC scanpath (ours)	0.196	0.836
CC scanpath + <i>WS-Saliency</i> (ours)	0.190	0.858
CC saliency/scanpath + <i>WS-Saliency</i> (ours)	0.231	0.857

to its original image resolution for evaluation.

## 4.2. Model Training

We use Spotlight [45] as the base model and retrain it on a series of pre-training tasks, including Web/Mobile UI understanding and natural image captioning [15]. Subsequently, we fine-tune the entire model using Adafactor optimizer with a learning rate of 0.1, batch size of 128, and image resolution of  $512 \times 512$ . All images maintain their aspect ratio and are padded to fit the training resolution. The model uses ViT B16 as the vision encoder and T5 base as the Transformer encoder of the image and text tokens, resulting in a total of 848 million parameters. The model is implemented in JAX. We use 64 Google Cloud TPU v3 to train our model UniAR for 20k steps in 12 hours.

**Datasets mixture** As we are combining a series of public datasets, in every iteration, for all training datasets in Tab. 1, we employ a random sampling strategy that ensures an equal sampling rate across these datasets. This approach guarantees that each dataset has an equal probability of contributing a sample, irrespective of its sample volume.

## 4.3. Experiment Results

We present results of UniAR for predicting heatmaps, scanpath-sequences as well as ratings across domains and datasets in Tabs. 2 to 4, compared to baselines which are trained on a specific domain, task, or dataset.

**Heatmap prediction** Performance of UniAR across five benchmarks is shown in Tab. 2. Across these datasets, which vary in domains (e.g., natural scenes, web pages,

graphic designs) and tasks (e.g., heatmaps of attention, importance), UniAR achieves SOTA performance compared to strong baselines, and outperforms previous SOTA in many cases. On *Mobile UI* and *Imp1k* datasets, UniAR outperforms previous SOTA across every metric. Out of 30 metrics detailed in the table, UniAR achieves SOTA in 21 and the second best in 7. The improvements are especially noteworthy in certain metrics: for instance, there is a 19.31% enhancement in the NSS metric on *Mobile UI*, and a significant 41.04% reduction in RMSE on *Imp1k*.

**Scanpath prediction** In Tab. 3, scanpath-sequence prediction results are shown for two datasets, *COCO-Search18* [16] (scanpath in natural scenes for object searching), *WS-Scanpath* [11] (scanpath on web pages under free viewing). On both datasets, UniAR performs comparably to baselines, and further outperforms baselines on all metrics on *WS-Scanpath*. Among 13 reported metrics in Tab. 3, our model achieved SOTA in 11, and second best in 1.

**Score prediction** In Tab. 4, we present rating prediction results on two subjective rating datasets: *KonIQ-10k* [30] on natural images and *Web Aesthetics* [22] on web pages. UniAR achieves the best results for PLCC metrics on both datasets and second best for SRCC on *KonIQ-10k*. Note that in Ke et al. [36], a multi-scale version of MUSIQ performs slightly better than ours on SRCC (0.916 vs 0.905). However, since our model does not use multi-scale image inputs, we did not include those results in our comparison.

**Visualizations** We present visualization results from UniAR on saliency/importance heatmap, scanpath, and ratings in Fig. 2 and Appendix C, compared to ground-truth.

## 4.4. Transferring Knowledge between Tasks

In this section, we demonstrate the zero-shot generalization ability between image domains and tasks of UniAR. Here, zero-shot generalization refers to a model’s ability to perform on completely unseen image domain and prediction tasks without requiring dedicated training. The experiment is designed to train our model on tasks and image domains with relevance, and evaluate the model on an entirely new combination of image domain and prediction task.

**Settings** Our experiment uses *WS* (web page) and *COCO-Freeview* (natural scene) datasets. We assess our model on scanpath prediction on the *WS-Scanpath* dataset. We vary the training sets in three different scenarios: (1) Using scanpath data from *COCO-Freeview*; (2) Combining scanpath data from *COCO-Freeview* with saliency heatmaps from *WS*; (3) Employing both scanpath and saliency heatmap data from *COCO-Freeview*, augmented with saliency heatmap data from *WS*. Each scenario maintains some relevance to our test set by either sharing the same prediction task or image domain, but never both.

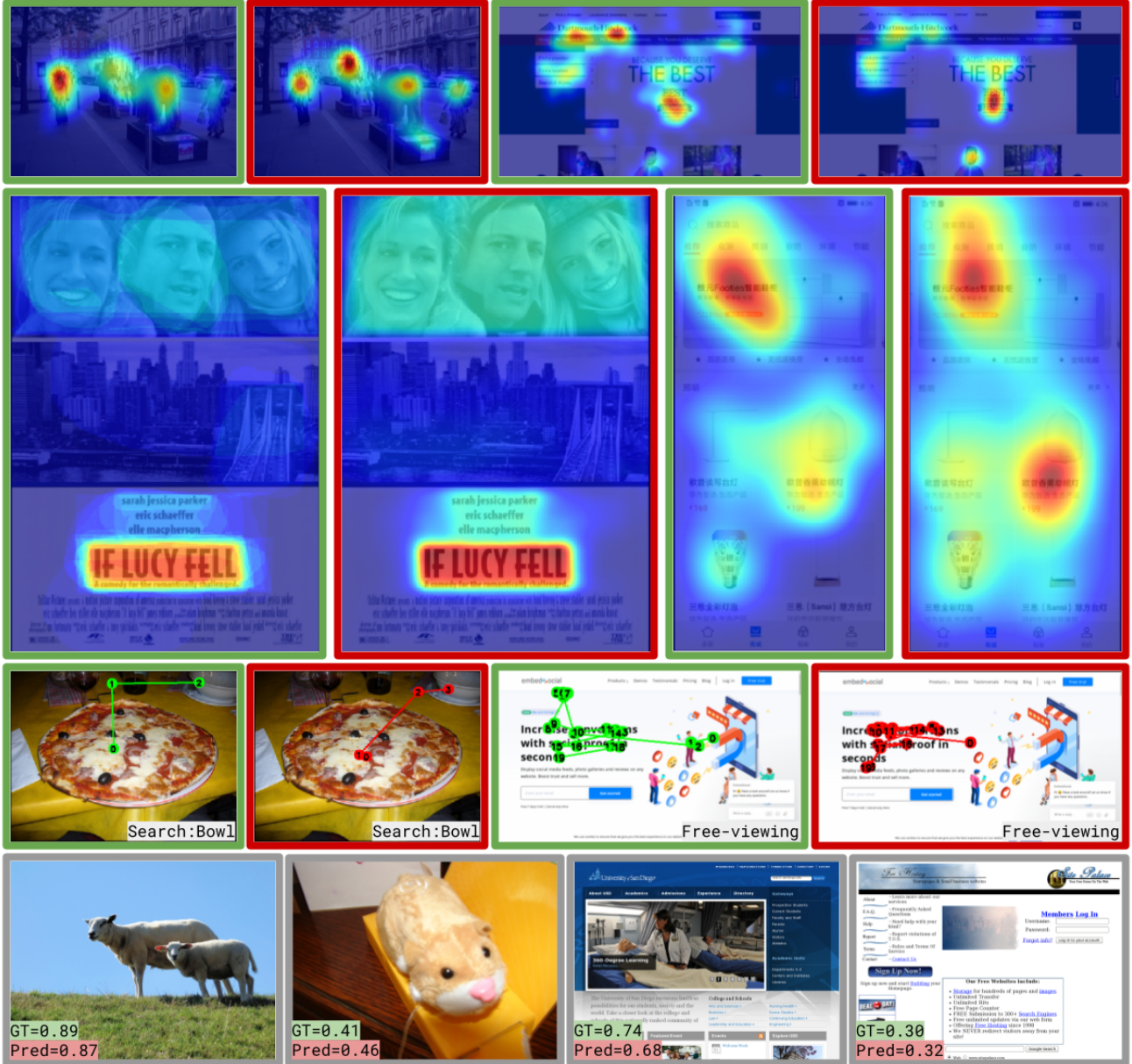


Figure 2. Visualizations on UniAR’s predictions. Images in green border or numbers in green are ground-truth, while images in red border or numbers in red are UniAR’s predictions. **First row:** saliency heatmap on *Salicon* and *WS-Saliency* dataset. **Second row:** importance heatmap on *ImpIk* dataset, and saliency heatmap on *Mobile UI* dataset. **Third row:** object-searching scanpath and free-viewing scanpath on *COCO-Search18* and *WS-Scanpath* dataset. **Fourth row:** rating prediction on *Koniq-10k* and *Web Aesthetics* datasets.

**Observations** In Tab. 5, we show experimental results for the above scenarios, and also attach the previous SOTA results on this testing set and the results from UniAR (full training data) as reference. As shown in the table, our third scenario: leveraging scanpath and saliency heatmap from *COCO-Freeview* and saliency heatmap from *WS*, showing promising results against previous numbers from [11], despite the model not having access to web page scanpath data. Using saliency heatmap as a *bridge*, showcasing the scanpath in natural scene data, and sharing task informa-

tion via text prompts, the model generalized reasonably well to an unseen domain-task combination. However, the performance does not match the previous results from UniAR, which is understandable due to the lack of training samples. Prediction performance declines in scenarios 1 and 2, which use more limited datasets, but remains competitive.

This ability to transfer and generalize knowledge from data in a zero-shot setting highlights a significant advantage of our proposed task unification approach. It is particularly beneficial for novel applications where obtaining

labeled data for specific domains and tasks may be challenging, but only related domain or task data is available.

## 5. Conclusion

In this paper, we developed a multimodal, unified model UniAR to predict implicit and explicit human behaviors on visual content, ranging from human attention to subjective ratings/preferences using image-text prompts. This model, trained on diverse public datasets across digital designs and natural scene images, effectively predicts human attention heatmaps, scanpath sequences, and subjective ratings such as aesthetic/quality scores. Our model achieves SOTA performance across multiple benchmarks and tasks.

**Ethical conduct** In our experiments, we incorporate data derived from human subjects which is obtained through user studies and interactions with individuals. We strictly adhere to ethical guidelines by ensuring that all data used by our model is public and devoid of any personal or sensitive information about individuals. Our model is designed not to utilize any sensitive information or individual identification, and eschews any form of personalization. This approach aligns with general ethical conduct, safeguarding against privacy issues when deploying our model.

## References

- [1] Kfir Aberman, Junfeng He, Yossi Gadsman, Inbar Mosseri, David E Jacobs, Kai Kohlhoff, Yael Pritch, and Michael Rubinstein. Deep saliency prior for reducing visual distraction. In *Proceedings of the IEEE/CVF Conference on Computer Vision and Pattern Recognition*, 2022. 1
- [2] Hossein Adeli, Françoise Vitu, and Gregory J Zelinsky. A model of the superior colliculus predicts fixation locations during scene viewing and visual search. *Journal of Neuroscience*, 2017. 6
- [3] Rohan Anil, Andrew M Dai, Orhan Firat, Melvin Johnson, Dmitry Lepikhin, Alexandre Passos, Siamak Shakeri, Emanuel Taropa, Paige Bailey, Zhifeng Chen, et al. Palm 2 technical report. *arXiv preprint arXiv:2305.10403*, 2023. 3
- [4] Saskia Bakker and Karin Niemantsverdriet. The interaction-attention continuum: Considering various levels of human attention in interaction design. *International Journal of Design*, 2016. 1
- [5] Leonardo Bonanni, Chia-Hsun Lee, and Ted Selker. Attention-based design of augmented reality interfaces. In *CHI'05 extended abstracts on Human factors in computing systems*, 2005. 1
- [6] Ali Borji, Hamed R Tavakoli, Dicky N Sihite, and Laurent Itti. Analysis of scores, datasets, and models in visual saliency prediction. In *Proceedings of the IEEE International Conference on Computer Vision*, 2013. 5
- [7] Sebastian Bosse, Dominique Maniry, Klaus-Robert Müller, Thomas Wiegand, and Wojciech Samek. Deep neural networks for no-reference and full-reference image quality assessment. *IEEE Transactions on image processing*, 2017. 7
- [8] Zoya Bylinskii, Nam Wook Kim, Peter O'Donovan, Sami Alsheikh, Spandan Madan, Hanspeter Pfister, Fredo Durand, Bryan Russell, and Aaron Hertzmann. Learning visual importance for graphic designs and data visualizations. In *Proceedings of the 30th Annual ACM Symposium on User Interface Software and Technology*, 2017. 6
- [9] Zoya Bylinskii, Nam Wook Kim, Peter O'Donovan, Sami Alsheikh, Spandan Madan, Hanspeter Pfister, Frédo Durand, Bryan C. Russell, and Aaron Hertzmann. Learning visual importance for graphic designs and data visualizations. *Proceedings of the 30th Annual ACM Symposium on User Interface Software and Technology*, 2017. 1
- [10] Zoya Bylinskii, Tilke Judd, Aude Oliva, Antonio Torralba, and Frédo Durand. What do different evaluation metrics tell us about saliency models? *IEEE Transactions on Pattern Analysis and Machine Intelligence*, 2018. 5
- [11] Souradeep Chakraborty, Zijun Wei, Conor Kelton, Seoyoung Ahn, Aruna Balasubramanian, Gregory J Zelinsky, and Dimitris Samaras. Predicting visual attention in graphic design documents. *IEEE Transactions on Multimedia*, 2022. 1, 5, 6, 7, 8
- [12] Shi Chen, Nachiappan Valliappan, Shaolei Shen, Xinyu Ye, Kai Kohlhoff, and Junfeng He. Learning from unique perspectives: User-aware saliency modeling. In *Proceedings of the IEEE/CVF Conference on Computer Vision and Pattern Recognition*, 2023. 2, 5, 6
- [13] Ting Chen, Saurabh Saxena, Lala Li, Tsung-Yi Lin, David J Fleet, and Geoffrey E Hinton. A unified sequence interface for vision tasks. *Advances in Neural Information Processing Systems*, 2022. 4
- [14] Xianyu Chen, Ming Jiang, and Qi Zhao. Predicting human scanpaths in visual question answering. In *Proceedings of the IEEE/CVF Conference on Computer Vision and Pattern Recognition*, 2021. 2, 6
- [15] Xi Chen, Xiao Wang, Soravit Changpinyo, AJ Piergiovanni, Piotr Padlewski, Daniel Salz, Sebastian Goodman, Adam Grycner, Basil Mustafa, Lucas Beyer, Alexander Kolesnikov, Joan Puigcerver, Nan Ding, Keran Rong, Hassan Akbari, Gaurav Mishra, Linting Xue, Ashish Thapliyal, James Bradbury, Weicheng Kuo, Mojtaba Seyedhosseini, Chao Jia, Burcu Karagol Ayan, Carlos Riquelme, Andreas Steiner, Anelia Angelova, Xiaohua Zhai, Neil Houlsby, and Radu Soricut. Pali: A jointly-scaled multilingual language-image model, 2022. 3, 7
- [16] Yupei Chen, Zhibo Yang, Seoyoung Ahn, Dimitris Samaras, Minh Hoai, and Gregory Zelinsky. Coco-search18 fixation dataset for predicting goal-directed attention control. *Scientific Reports*, 2021. 5, 6, 7
- [17] Yupei Chen, Zhibo Yang, Souradeep Chakraborty, Sounak Mondal, Seoyoung Ahn, Dimitris Samaras, Minh Hoai, and Gregory Zelinsky. Characterizing target-absent human attention. In *Proceedings of the IEEE/CVF Conference on Computer Vision and Pattern Recognition*, 2022. 2
- [18] Hyung Won Chung, Le Hou, Shayne Longpre, Barret Zoph, Yi Tay, William Fedus, Yunxuan Li, Xuezhi Wang, Mostafa Dehghani, Siddhartha Brahma, et al. Scaling instruction-finetuned language models. *arXiv preprint arXiv:2210.11416*, 2022. 3
- [19] Marcella Cornia, Lorenzo Baraldi, Giuseppe Serra, and Rita Cucchiara. Predicting Human Eye Fixations via an LSTM-based Saliency Attentive Model. *IEEE Transactions on Image Processing*, 2018. 2, 6
- [20] Filipe Cristina, Sebastiaan Mathôt, Jan Theeuwes, and Iain D Gilchrist. Scanmatch: A novel method for comparing fixation sequences. *Behavior Research Methods*, 2010. 1
- [21] Benjamin de Haas, Alexios L. Iakovidis, D. Samuel Schwarzkopf, and Karl R. Gegenfurtner. Individual differences in visual salience vary along semantic dimensions. *Proceedings of the National Academy of Sciences*, 2019. 1
- [22] Alexandros Delitzas, Kyriakos C Chatzidimitriou, and Andreas L Symeonidis. Calista: A deep learning-based system for understanding and evaluating website aesthetics. *International Journal of Human-Computer Studies*, 2023. 5, 7
- [23] Richard Dewhurst, Marcus Nyström, Halszka Jarodzka, Tom Foulsham, Roger Johansson, and Kenneth Holmqvist. It depends on how you look at it: Scanpath comparison in multiple dimensions with multimap, a vector-based approach. *Behavior Research Methods*, 2012. 1, 5
- [24] Alexey Dosovitskiy, Lucas Beyer, Alexander Kolesnikov, Dirk Weissenborn, Xiaohua Zhai, Thomas Unterthiner, Mostafa Dehghani, Matthias Minderer, Georg Heigold, Sylvain Gelly, Jakob Uszkoreit, and Neil Houlsby. An image is

worth 16x16 words: Transformers for image recognition at scale. In *ICLR*, 2021. 3

[25] Camilo Fosco, Vincent Casser, Amish Kumar Bedi, Peter O’Donovan, Aaron Hertzmann, and Zoya Bylinskii. Predicting visual importance across graphic design types. In *Proceedings of the 33rd Annual ACM Symposium on User Interface Software and Technology*, 2020. 4, 5, 6

[26] Camilo Fosco, Vincent Casser, Amish Kumar Bedi, Peter O’Donovan, Aaron Hertzmann, and Zoya Bylinskii. Predicting visual importance across graphic design types. In *Proceedings of the 33rd Annual ACM Symposium on User Interface Software and Technology*, page 249–260, 2020. 1

[27] Jonathan Harel, Christof Koch, and Pietro Perona. Graph-based visual saliency. *Advances in Neural Information Processing Systems*, 2006. 6

[28] Sen He, Hamed R Tavakoli, Ali Borji, Yang Mi, and Nicolas Pugeault. Understanding and visualizing deep visual saliency models. In *Proceedings of the IEEE/CVF Conference on Computer Vision and Pattern Recognition*, 2019. 6

[29] Weng Khuan Hoh, Fang-Lue Zhang, and Neil A Dodgson. Salient-centeredness and saliency size in computational aesthetics. *ACM Transactions on Applied Perception*, 2023. 1

[30] Vlad Hosu, Hanhe Lin, Tamas Sziranyi, and Dietmar Saupe. Koniq-10k: An ecologically valid database for deep learning of blind image quality assessment. *IEEE Transactions on Image Processing*, 2020. 5, 7

[31] Feiyan Hu and Kevin McGuinness. Fastsal: a computationally efficient network for visual saliency prediction. In *2020 25th International Conference on Pattern Recognition (ICPR)*. IEEE, 2021. 6

[32] Laurent Itti, Christof Koch, and Ernst Niebur. A model of saliency-based visual attention for rapid scene analysis. *IEEE Transactions on Pattern Analysis and Machine Intelligence*, 1998. 6

[33] Sen Jia and Neil DB Bruce. Eml-net: An expandable multi-layer network for saliency prediction. *Image and Vision Computing*, 2020. 2, 6

[34] Ming Jiang, Shengsheng Huang, Juanyong Duan, and Qi Zhao. Salicon: Saliency in context. In *Proceedings of the IEEE Conference on Computer Vision and Pattern Recognition*, 2015. 5, 6

[35] Tilke Judd, Krista Ehinger, Frédo Durand, and Antonio Torralba. Learning to predict where humans look. In *IEEE International Conference on Computer Vision*, 2009. 5

[36] Junjie Ke, Qifei Wang, Yilin Wang, Peyman Milanfar, and Feng Yang. Musiq: Multi-scale image quality transformer. In *Proceedings of the IEEE/CVF International Conference on Computer Vision*, 2021. 3, 5, 7

[37] Jongyoo Kim and Sanghoon Lee. Fully deep blind image quality predictor. *IEEE Journal of selected topics in signal processing*, 2016. 7

[38] Solomon Kullback. *Information theory and statistics*. Courier Corporation, 1997. 5

[39] Matthias Kümmerer, Thomas SA Wallis, and Matthias Bethge. Deepgaze ii: Reading fixations from deep features trained on object recognition. *arXiv preprint arXiv:1610.01563*, 2016. 6

[40] Matthias Kümmerer, Thomas SA Wallis, Leon A Gatys, and Matthias Bethge. Understanding low-and high-level contributions to fixation prediction. In *Proceedings of the IEEE International Conference on Computer Vision*, 2017. 2

[41] Olivier Le Meur, Patrick Le Callet, and Dominique Barba. Predicting visual fixations on video based on low-level visual features. *Vision Research*, 2007. 5

[42] Luis A Leiva, Yunfei Xue, Avya Bansal, Hamed R Tavakoli, Tuğçe Körülü, Jingzhou Du, Niraj R Dayama, and Antti Oulasvirta. Understanding visual saliency in mobile user interfaces. In *22nd International Conference on Human-Computer Interaction with Mobile Devices and Services*, 2020. 1, 5, 6

[43] Vladimir I Levenshtein et al. Binary codes capable of correcting deletions, insertions, and reversals. In *Soviet Physics Doklady*. Soviet Union, 1966. 5

[44] Dingquan Li, Tingting Jiang, Weisi Lin, and Ming Jiang. Which has better visual quality: The clear blue sky or a blurry animal? *IEEE Transactions on Multimedia*, 2018. 7

[45] Gang Li and Yang Li. Spotlight: Mobile ui understanding using vision-language models with a focus. *arXiv preprint arXiv:2209.14927*, 2022. 3, 4, 7

[46] Alaster J Meehan and Joanne B Culpepper. Clutter estimation and perception. *Optical Engineering*, 2016. 1

[47] Anish Mittal, Anush Krishna Moorthy, and Alan Conrad Bovik. No-reference image quality assessment in the spatial domain. *IEEE Transactions on image processing*, 2012. 2, 7

[48] Sounak Mondal, Zhibo Yang, Seoyoung Ahn, Dimitris Samaras, Gregory Zelinsky, and Minh Hoai. Gazeformer: Scalable, effective and fast prediction of goal-directed human attention. In *Proceedings of the IEEE/CVF Conference on Computer Vision and Pattern Recognition*, 2023. 2, 4, 5, 6, 1

[49] Bence Nanay. Aesthetic attention. *Journal of Consciousness Studies*, 2015. 1

[50] Saul B Needleman and Christian D Wunsch. A general method applicable to the search for similarities in the amino acid sequence of two proteins. *Journal of Molecular Biology*, 1970. 5

[51] OpenAI. Gpt-4 technical report, 2023. 3

[52] Junting Pan, Cristian Canton Ferrer, Kevin McGuinness, Noel E O’Connor, Jordi Torres, Elisa Sayrol, and Xavier Giro-i Nieto. Salgan: Visual saliency prediction with generative adversarial networks. *arXiv preprint arXiv:1701.01081*, 2017. 6

[53] Robert J Peters, Asha Iyer, Laurent Itti, and Christof Koch. Components of bottom-up gaze allocation in natural images. *Vision Research*, 2005. 5

[54] Colin Raffel, Noam Shazeer, Adam Roberts, Katherine Lee, Sharan Narang, Michael Matena, Yanqi Zhou, Wei Li, and Peter J. Liu. Exploring the limits of transfer learning with a unified text-to-text transformer, 2023. 3

[55] Navyasri Reddy, Samyak Jain, Pradeep Yarlagadda, and Vineet Gandhi. Tidying deep saliency prediction architectures. In *2020 IEEE/RSJ International Conference on Intelligent Robots and Systems*, 2020. 2, 5, 6

[56] Claudia Roda. Human attention and its implications for human–computer interaction. *Human attention in digital environments*, 2011. 1

[57] Yossi Rubner, Carlo Tomasi, and Leonidas J Guibas. The earth mover’s distance as a metric for image retrieval. *International Journal of Computer Vision*, 2000. 5

[58] Eldon Schoop, Xin Zhou, Gang Li, Zhourong Chen, Bjoern Hartmann, and Yang Li. Predicting and explaining mobile ui tappability with vision modeling and saliency analysis. In *Conference on Human Factors in Computing Systems (CHI)*, 2022. 1

[59] Lisa Schwetlick, Lars Oliver Martin Rothkegel, Hans Arne Trukenbrod, and Ralf Engbert. Modeling the effects of perisaccadic attention on gaze statistics during scene viewing. *Communications Biology*, 2020. 6

[60] Chengyao Shen and Qi Zhao. Webpage saliency. In *Proceedings of the European Conference on Computer Vision*, 2014. 1, 5, 6

[61] Shaolin Su, Qingsen Yan, Yu Zhu, Cheng Zhang, Xin Ge, Jinqiu Sun, and Yanning Zhang. Blindly assess image quality in the wild guided by a self-adaptive hyper network. In *Proceedings of the IEEE/CVF Conference on Computer Vision and Pattern Recognition*, 2020. 3, 7

[62] Nachiappan Valliappan, Na Dai, Ethan Steinberg, Junfeng He, Kantwon Rogers, Venky Ramachandran, Pingmei Xu, Mina Shojaeizadeh, Li Guo, Kai Kohlhoff, et al. Accelerating eye movement research via accurate and affordable smartphone eye tracking. *Nature Communications*, 2020. 6

[63] Ronald Van den Berg, Frans W Cornelissen, and Jos BTM Roerdink. A crowding model of visual clutter. *Journal of Vision*, 2009. 1

[64] Wenguan Wang and Jianbing Shen. Deep visual attention prediction. *IEEE Transactions on Image Processing*, 2017. 6

[65] Juan Xu, Ming Jiang, Shuo Wang, Mohan S Kankanhalli, and Qi Zhao. Predicting human gaze beyond pixels. *Journal of Vision*, 2014. 5

[66] Jingtao Xu, Peng Ye, Qiaohong Li, Haiqing Du, Yong Liu, and David Doermann. Blind image quality assessment based on high order statistics aggregation. *IEEE Transactions on Image Processing*, 2016. 7

[67] Sheng Yang, Guosheng Lin, Qiuping Jiang, and Weisi Lin. A dilated inception network for visual saliency prediction. *IEEE Transactions on Multimedia*, 2019. 6

[68] Zhibo Yang, Lihan Huang, Yupei Chen, Zijun Wei, Seoyoung Ahn, Gregory Zelinsky, Dimitris Samaras, and Minh Hoai. Predicting goal-directed human attention using inverse reinforcement learning. In *Proceedings of the IEEE/CVF Conference on Computer Vision and Pattern Recognition*, 2020. 2, 6

[69] Zhibo Yang, Sounak Mondal, Seoyoung Ahn, Gregory Zelinsky, Minh Hoai, and Dimitris Samaras. Target-absent human attention. In *Proceedings of the European Conference on Computer Vision*, 2022. 2, 5, 6

[70] Chen-Ping Yu, Dimitris Samaras, and Gregory J Zelinsky. Modeling visual clutter perception using proto-object segmentation. *Journal of vision*, 2014. 1

[71] Dario Zanca, Stefano Melacci, and Marco Gori. Gravitational laws of focus of attention. *IEEE Transactions on Pattern Analysis and Machine Intelligence*, 2019. 6

[72] Hui Zeng, Lei Zhang, and Alan C Bovik. A probabilistic quality representation approach to deep blind image quality prediction. *arXiv preprint arXiv:1708.08190*, 2017. 7

[73] Jianming Zhang and Stan Sclaroff. Saliency detection: A boolean map approach. In *Proceedings of the IEEE International Conference on Computer Vision*, 2013. 6

[74] Lin Zhang, Lei Zhang, and Alan C Bovik. A feature-enriched completely blind image quality evaluator. *IEEE Transactions on Image Processing*, 2015. 2, 7

[75] Weixia Zhang, Kede Ma, Jia Yan, Dexiang Deng, and Zhou Wang. Blind image quality assessment using a deep bilinear convolutional neural network. *IEEE Transactions on Circuits and Systems for Video Technology*, 2018. 3, 7

[76] Quanlong Zheng, Jianbo Jiao, Ying Cao, and Rynson WH Lau. Task-driven webpage saliency. In *Proceedings of the European Conference on Computer Vision*, 2018. 1, 6

[77] Hancheng Zhu, Leida Li, Jinjian Wu, Weisheng Dong, and Guangming Shi. Metaiqa: Deep meta-learning for no-reference image quality assessment. In *Proceedings of the IEEE/CVF Conference on Computer Vision and Pattern Recognition*, 2020. 7

# UniAR: Unifying Human Attention and Response Prediction on Visual Content

## Supplementary Material

### A. Model Details

The main model components consist of a ViT B16 encoder for image encoding, a T5 base encoder for mixing image and text tokens, and three predictors for rating, heatmap, and scanpath prediction, respectively.

**Vision Transformer and T5 Encoder** The ViT B16 encoder uses  $16 \times 16$  patch size, 12 layers with 12 heads, MLP dimension 3,072, and hidden dimension 768. The T5 base encoder uses 12 layers with 12 heads and MLP dimension 2,048 and hidden dimension 768.

**Score Predictor** The score predictor consists of four convolutional layers with Layer Normalization and ReLU activation. The filter size, kernel size, and strides are  $[768, 384, 128, 64], [2, 2, 2, 2], [1, 1, 1, 1]$ , respectively. Three dense layers of size 2,048, 1,024 and 1 are used to generate a scalar with ReLU activations for the first two layers, and sigmoid for the last.

**Heatmap Predictor** The heatmap predictor consists of two convolution layers with filter size, kernel size, and stride as  $[768, 384], [3, 3], [1, 1]$ , respectively. It then uses four de-convolution layers to up-sample to the required output resolution, with the filter size, kernel size, and stride as  $[768, 384, 384, 192], [3, 3, 3, 3], [2, 2, 2, 2]$ , respectively. Each de-convolution layer is with two read-out convolution layers of kernel size 3 and stride 1. Layer Normalization and ReLU are used for each layer. In the end, two read-out convolution layers and a final sigmoid activation are used to generate the heatmap prediction.

**Scanpath Predictor** The scanpath predictor is implemented using a T5 base decoder with 12 layers of 12 heads and MLP dimension 2,048 and hidden dim 768. Output token length is 64.

### B. Dataset Processing

In this section, we describe some of the key dataset processing details.

**Imp1k** In the *Imp1k* dataset, we observe some resolution mismatch between the image and its ground-truth importance map. To unify the image and the ground-truth into the same resolution, we find out the lower resolution (with a smaller area) between these two and downsample the larger one into the lower resolution.

**WS-Scanpath** We asked Chakraborty et al. [11] for their code on evaluating the scanpath, and follow them to Mean-Shift clustering to generate spatial bins for the metric **SequenceScore**. We also follow their criteria to select the

number of clusters in MeanShift clustering which will be used in the evaluation later on.

**Mobile UI** We contacted the authors but the original dataset partition is missing. We randomly partitioned the dataset into a training and a testing set with the number of instances following Leiva et al. [42]. We calculate the saliency results using images without padding.

**COCO-Search18** For the scanpath results, we follow the updated experimental results in the appendix of GazeFormer [48]. The original results in the main paper are impacted by an image padding issue, as reported in their GitHub repo.

### C. More Visualizations

We attach another visualization of UniAR’s predictions in Fig. 3. UniAR offers consistently good predictions on three tasks across multiple datasets, compared to the ground-truths.

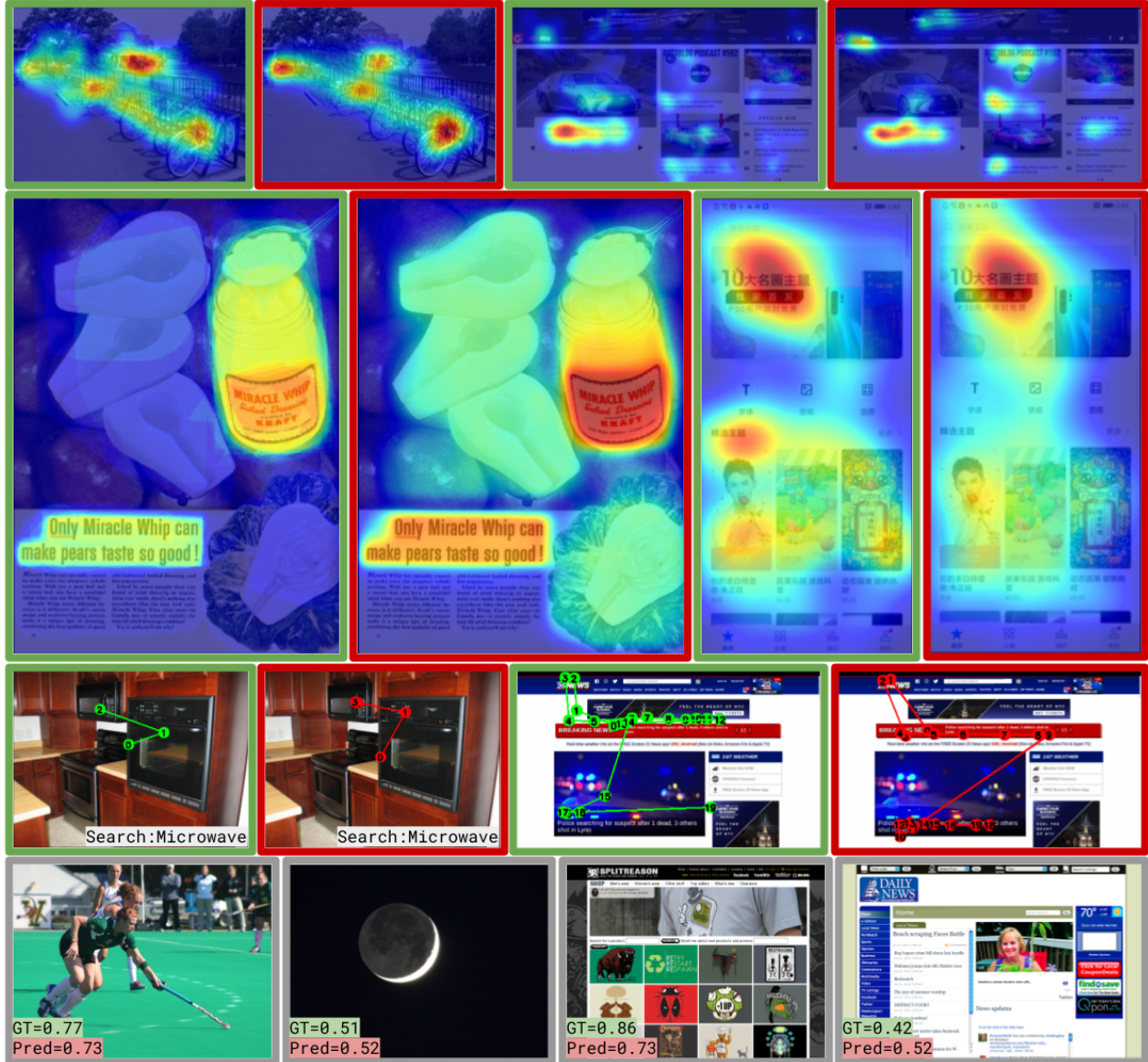


Figure 3. Another set of visualizations on UniAR’s predictions. Images in green border or numbers in green are ground-truth, while images in red border or numbers in red are UniAR’s predictions. **First row:** saliency heatmap on Salicon and WS-Saliency dataset. **Second row:** importance heatmap on Imp1k dataset, and saliency heatmap on Mobile UI dataset. **Third row:** object-searching scanpath and free-viewing scanpath on COCO-Search18 and WS-Scanpath dataset. **Fourth row:** rating prediction on KonIQ-10k and Web Aesthetics datasets.